

On the calibration of simplified vehicle crash models

Johannes Fender · Fabian Duddeck ·
Markus Zimmermann

Received: 10 October 2012 / Revised: 16 June 2013 / Accepted: 20 July 2013 / Published online: 30 August 2013
© Springer-Verlag Berlin Heidelberg 2013

Abstract Full-vehicle finite element models have a large number of degrees of freedom. This makes them ill suited for design work, numerical optimization or stochastic analyses in an early development phase, because they require a high level of detailed information, most of which is yet unavailable. They are also computationally expensive, thus severely limiting the number of function evaluations. Both difficulties can be alleviated through the use of substitute models, which capture only the relevant mechanisms, associated with a smaller number of degrees of freedom. This work provides a substitute modeling and calibration methodology which improves output value prediction for substantial deviations from the reference design, including three significant innovations. First, a new measure to quantify the agreement of calibrated and reference model is proposed. Second, a multi-model calibration is introduced, which incorporates an array of reference models for calibration and cross validation. Third, the calibration is performed on the basis of a hybrid objective function, weighting the agreement of the time dependent system states, called physics-based contribution, and the time independent output values, called predictive or regression-based. This ensures a large range of validity while simultaneously improving the

predictive quality of the model. It is also shown that the discretization of the structural mass has negligible influence on the target values, allowing for reduced model complexity.

Keywords Optimization · Surrogate model · Crashworthiness · Parameter identification · Model calibration · Lumped mass models

1 Introduction

Reduction of degrees of freedom In the design of automotive crash structures, the use of full vehicle finite element simulations is commonplace. These models have a high number of degrees of freedom. In crash simulation in a late development phase, such level of detail is necessary because the behavior of the vehicle structure is highly non-linear and crash performance depends on many geometric details, e.g. holes, spot welds, corrugations or stiffening plates. The high number of degrees of freedom of the full vehicle finite element model allows for an accurate representation of the crash at the cost of expensive computation and high modeling effort.

While well suited for later design stages, see Duddeck (2008), this is a disadvantage at early design stages, because the detail information required for such a model is not yet available. This results in misleadingly accurate simulations, because detail information, with high impact on the crash performance, is used which does not correspond to the future vehicle. This can be avoided by using substitute models which only incorporate the information available at the given design stage or data on the component performances (as opposed to design details) which will be realized.

Optimization with detail parameters is difficult. The degrees of freedom of a finite element model are nodal

J. Fender (✉) · M. Zimmermann
BMW Group, Research and Innovation Center,
Knorrstr. 147, 80937 Munich, Germany
e-mail: johannes.fender@bmw.de

M. Zimmermann
e-mail: markus.mz.zimmermann@bmw.de

F. Duddeck
Technische Universität München, Arcisstr. 21,
80333 München, Germany
e-mail: duddeck@tum.de

coordinates and material properties. Nodal coordinates are unsuited for direct numerical optimization or stochastic analyses. Higher level parametrization, i.e. defining new parameters which represent the position of sets of nodes, e.g. a corrugation or stiffening plate, is needed. Otherwise, most parameter variations result in infeasible or numerically unstable solutions, e.g. due to mesh distortion. Furthermore, because details such as geometry and material are yet to be defined, any result generated in terms of the structure's geometric detail is subject to change at a later design stage. This renders the results of the earlier optimization obsolete. Therefore, it is advantageous to not only use models with less parameters but also, to describe the crash performance in terms of functional parameters which are independent of any specific implementation.

Such a set of parameters are the functional properties of the structure. Functional properties describe what the component *does* in the system. E.g., the component does exert a specific force during compression. Opposed to that, non-functional properties describe what the component *is*, including, e.g., geometric detail or practicability, and may constrain the implementation. The concept of functional properties and requirements is essential in systems engineering and, e.g., illustrated in Wieggers (2003). For a USNCAP type front crash (for details see Section 2), suitable functional properties of the structural components are their force-deformation characteristics, as they are sufficient to describe the crash performance, measured by the vehicle acceleration, energy absorption and deformation, see Section 3.

Such a modeling approach is particularly applicable during the early development phase, when analyses have to be performed without complete geometry information and when short response times are required. Also, the role of the methods proposed in this work is in design goal definition. During product development, a phase of design goal definition is followed by integration and finally validation. During validation, detailed FE-simulations and laboratory tests are used to verify that the design fulfills the specified goals. Because the implementation of the detailed design depends on the design goals, the detail information cannot be available during design goal definition. This is, why modeling approaches which work with minimal detail information are necessary during the early development phase, up to the point where only validation is necessary.

State of the art The use of lumped mass models, such as in Kamal (1970), precedes FEM by more than a decade in crash analysis. In this approach, models consist of masses connected by springs. The linear spring stiffnesses are determined by component tests in the laboratory. The first approaches using spring elements with nonlinear characteristics were made in 1986 (Hollowell 1986). The nonlinear

behavior is approximated by piecewise linear functions where each linear step is assigned a sub domain in the time domain. In all cases, the parameter identification problem is solved via numerical optimization algorithms with the goal of matching either kinematic and kinetic behavior or eigenvalues and eigenvectors of the system, depending on the problem, to a reference system.

In Markiewicz et al. (2001), rigid elements and non-linear beam elements are used in addition to spring elements to simulate the behavior of a railway driver's cabin. Here, element parameters are obtained from static experiments and kinematic models.

Cornette et al. (1997) obtain spring characteristics, using three-dimensional kinematic models as well. These models are used to analytically calculate the resistance to collapse for thin-walled structures of arbitrary prismatic geometry. The assumed underlying mechanism is plastic hinging. The plastic hinge approach was presented as early as 1983 by Nikravesh et al. (1983), with spring characteristics obtained from experimental results. The results are then used in multi body models. Multi body modeling approaches are discussed in Pereira and Ambrósio (1997) as well, here with a focus on railway cars, using a hybrid approach between component and structure based characteristics, also obtained experimentally. A similar approach is pursued in Halgrin et al. (2008), with a focus on optimization of spring localization and characteristics with respect to computational performance.

In the definition of the objective function, the use of L_1 , L_2 and L_∞ norms has been discussed exhaustively. Kim and Arora (2001) should be consulted for an in depth summary of the work done in the field up to the year 2001 and works on parametric and nonparametric system identification problems for lumped mass models in crashworthiness optimization in Kim et al. (2001).

Since then, approaches in the direction of multi-body simulations for crashworthiness were made, see Carvalho et al. (2011) and Sousa et al. (2008). Particularly in Sousa et al. (2008), simplified models, based on the plastic hinge multi body approach, are calibrated to represent a full vehicle finite element model. As with this work, the goal is to obtain an as realistic as possible crash response with a minimum of detail information. The type of model used in this work is based on the load path concept model, developed by Kerstan and Bartelheimer, see Kerstan and Bartelheimer (2011).

Multi-model calibration Lumped mass models are a common substitute modeling technique in vehicle crash design, see, e.g., Huang (2002). The vehicle structure is represented by discrete force elements which are connected at nodes. The nodes carry the vehicle's mass. Interaction of the elements and masses is described through the element's

force-deformation characteristic. Usually such models are initially calibrated with respect to a single reference detail model. The substitute model’s parameters are chosen such that its output variables agree with the detail model. This does not necessarily imply that this agreement in the output variables persists through changes in both model’s design parameters. In order to ensure good output value prediction, an approach is presented, in which calibration is simultaneously performed on an array of substitute models and reference models. Optimization algorithms are used to find a set of calibration parameters, which provides the best overall fit to the reference systems, given varying design parameters. The calibration is cross validated against a second array of substitute and reference systems, in order to ensure that unfamiliar designs are still correctly represented by the substitute model.

Hybrid objective function A hybrid objective function is used, that allows for weighted evaluation of the agreement of the system’s time dependent physical states and the time independent output values. Good agreement in the system’s physical states improves robustness because the underlying mechanisms of the structure are captured well, thus reflecting the influence of changes in design variables realistically. Considering the integrated output values, which are the values the user is ultimately interested in, during calibration, however, improves the predictive quality of the model because integrated errors over the system’s states are weighted separately and directly penalized.

2 Problem

In the USNCAP front crash load case, the test vehicle is driven against a rigid barrier at full overlap with an initial velocity of $56 \frac{km}{h}$. The criteria for the USNCAP crash load case in the laboratory are evaluated using values measured with a crash test dummy, e.g. head acceleration, chest acceleration and deflection, neck moment and pelvis acceleration, see National Highway Traffic Safety Administration (2005). These values depend on the crash structure as well as the restraint systems.

The variable that describes the boundary condition for the restraint system design is the acceleration at the lower end of the B-pillar, see Huang (2002). In Fig. 1, the target values, i.e. the system’s quantities which are considered in the evaluation of a design, for USNCAP front crash structural design are shown. The vehicle structure is to be designed such that the filtered acceleration a at the B-pillar stays below a critical level, it is possible to design a restraint system which yields sub critical dummy values. Another goal is that no part of the firewall may intrude into the passenger cell past a certain threshold.

3 The simplified model

3.1 One-element model

Considering a one-dimensional load case where the load is symmetrical and unidirectional as for the USNCAP, only the accelerations, forces and displacements in the direction x are of interest. Therefore, a simplified model is used to predict the B-pillar x -acceleration and the firewall intrusions. This model is based on the main functional properties of the vehicle’s front structure, which are its *force-deformation characteristics*.

To explain the principle, a very simple model is regarded, based on a single degree of freedom system (Fig. 2). Here the vehicle is separated into two parts, the front structure which guarantees the energy absorption and the rear vehicular structure which is considered as a single mass m_{rv} .

This means that all degree of freedoms between barrier and firewall are neglected, leading to a one-dimensional scalar problem. $x_2, \dot{x}_2, \ddot{x}_2$ are the displacement, velocity and acceleration of the rear mass.

Then the section force across the entire front structure in the y - z -plane at the firewall (position B, see Fig. 2) is considered. Figure 2 gives a schematic drawing of a vehicle’s front structure, represented by one macro-element with the mass of the rear vehicle, m_{rv} , attached. The force F_B , measured directly in front of the firewall, determines the acceleration of the passenger cell.

$$m_{rv}\ddot{x}(t) = F(t) \tag{1}$$

Figure 2 is a schematic drawing of a vehicle’s front structure, represented by one macro-element with the mass of the rear vehicle, m_{rv} , attached. The force F_2 , measured directly in front of the fire wall, determines the acceleration of the passenger cell. The following assumptions are made regarding this macro-element:

- the macro-element is only subject to compression,
- elasticity is neglected,
- rate dependency is neglected.

Under these assumptions, the macro-element’s force response in the direction of x to a deformation $u = x_2 - x_1$ is given by

$$F_x = \hat{F}(u). \tag{2}$$

$\hat{F}(u)$ is the macro-element’s *force-deformation characteristic*, an arbitrary function of u . Note that the force only depends on the deformation. Thus, (1) is written as

$$m_{rv}\ddot{x}(t) = -\hat{F}(u(t)). \tag{3}$$

Local structural deformations and material behavior are completely represented by using force-deformation characteristics. For example, a beam that responds to compression

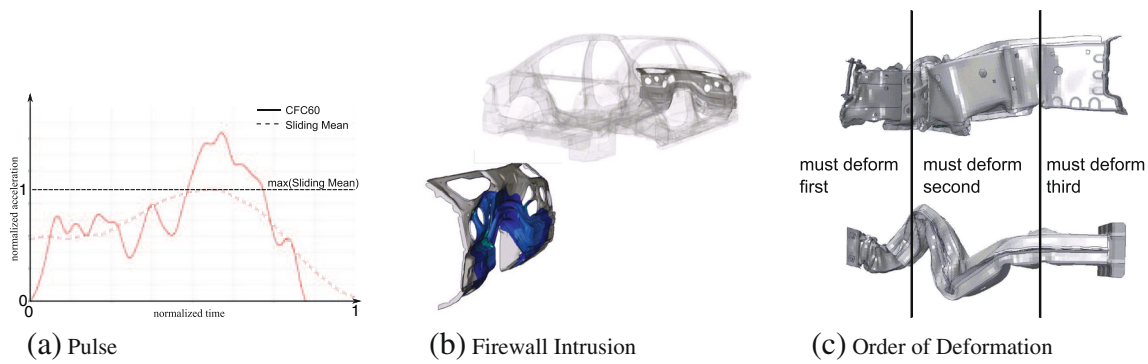


Fig. 1 Design goals for USNCAP crash structure design

with axial crushing has a different force-deformation characteristic than a beam that responds with buckling, see Fig. 3. The resulting acceleration at the end of the beam only depends on the force exerted by the element and not on whether this force is exerted during buckling or axial crushing. This also means, that this macro-element does not have any mechanical properties of its own but only mimics the one-dimensional force-deformation characteristic of the structure it represents. Thus, the length of such an element is equivalent to the length of the structure it represents. An increase in model detail using this approach is not accomplished by reducing element sizes, as in finite element analysis, but rather by increasing the detail of the force-deformation characteristics which are mapped onto the element.

3.2 Generalization: the structural model

Based on the assumption that any structure can be represented in this manner, i.e. an output acceleration only depending on the acting forces and decelerated mass, the front structure can be broken down into a network of elements and nodes. These load paths are connected only at the branching points of the structure, see Fig. 6. Each element is subject to the previous assumptions. In contrast to the

model with only one element, the newly introduced branching points may experience forces not only in the direction of x but also in y and z , because the actual deformation mechanisms of adjacent components may induce transverse forces. This has to happen in a moderate fashion. If lateral forces become too large, the deformation mode of adjacent components, and consequently their force-deformation-characteristic in x , may change. Breaking the front structure down into multiple components leads to a system of differential equations that is similar to (3). For any node A of the system, with the directly connected nodes B , the following holds:

$$m_A \begin{pmatrix} \ddot{x}_A \\ \ddot{y}_A \\ \ddot{z}_A \end{pmatrix} = \sum_B \begin{pmatrix} F_x(\mathbf{x}_B - \mathbf{x}_A) \\ F_y(\mathbf{x}_B - \mathbf{x}_A) \\ F_z(\mathbf{x}_B - \mathbf{x}_A) \end{pmatrix}. \tag{4}$$

m is the node’s mass, \mathbf{x}_A and \mathbf{x}_B , are the vectors of x , y , and z -positions of the nodes A and B and F_x , F_y and F_z are the forces acting on the node in x , y and z . Because the accelerations and deformations only depend on the forces in their respective directions and only \ddot{x} is of interest, transversal forces acting within the structure can be disregarded for the x -balance. Also, F_x is assumed to only depend on $x_B - x_A$ and not on the relative displacements in y and z . Thus, the system is reduced to

$$m_A \ddot{x}_A = \sum_B \hat{F}_x(x_B - x_A). \tag{5}$$

A force-deformation characteristic $\hat{F}_x(x_B - x_A) = \hat{F}_x(u)$ can be defined for each element connecting the node A to any of its adjacent nodes B , describing its reaction force in x only depending on the relative x -displacement of its end points, $u = x_B - x_A$, see Fig. 4. Note that in that respect, it is not necessary to know anything about the component except for its x -force-deformation characteristic. Material,

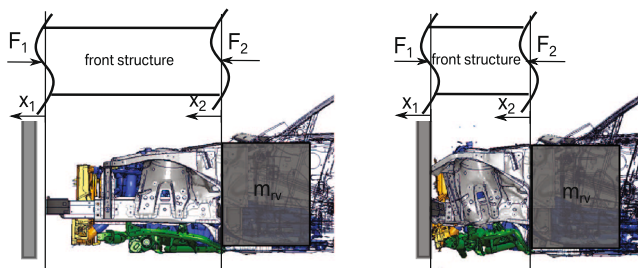
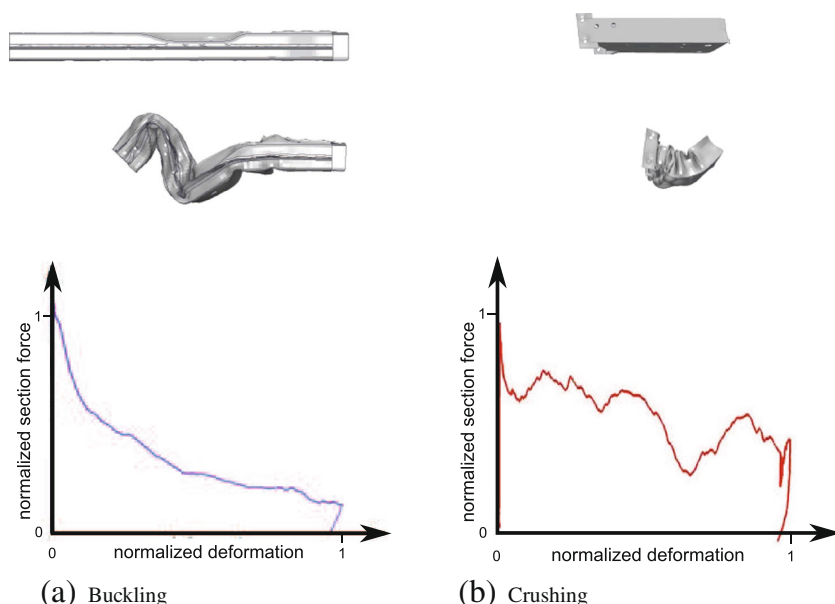


Fig. 2 Vehicle front structure with free body diagram, measuring the total force across the entire front structure

Fig. 3 Deformation and force-deformation characteristics of a beam element subject to buckling and axial crushing



deformation behavior, e.g. buckling, bending or total decomposition, are all included in the component’s force-deformation characteristic. Naturally, changes in these parameters, e.g. material or mode of deformation, will result in a different force-deformation characteristic.

Applicability to other load cases is limited. The approach is only suitable, if for all components the force F_x only depends on the relative displacement of the nodes of the component in the x -direction and only F_x and x are of interest. Both is true for the USNCAP and FMVSS regulations, where a front impact at ninety degrees with a rigid, stationary barrier is tested. Asymmetric or multi directional impacts such as the EuroNCAP type front crash include lateral deformations and forces which cannot be modeled using this approach. Also, the approach is only suited for modeling structures with distinct load paths but not for structures such as those used for deformable barriers in, e.g., the EuroNCAP type front crash or US side impact load cases.

3.3 Influence of component mass

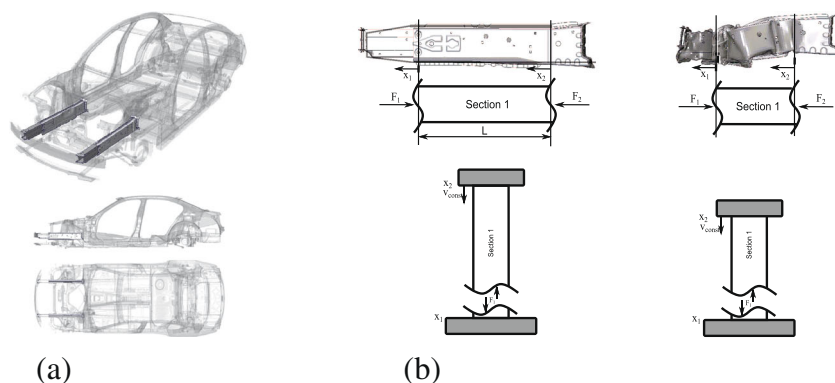
When measuring a component’s force-deformation characteristic in a high velocity crash load case, two effects which produce an error occur.

The first effect is, that during deformation of the component, more and more of the components mass is abruptly brought from a higher velocity to a lower velocity in the zone of high local deformation.

The second effect is, that the component’s mass, which, as a whole, is decelerated as well, acts upon the section force. The magnitude of the effect depends on the x -position along the component where the section force is measured.

When representing a component, which has a continuous distribution of mass, using a simplified element with discrete masses, the total error depends on where the section force was measured in the reference model and how the discrete masses are distributed along the substitute element.

Fig. 4 Component in a vehicle structure (a) and in a test stand (b)



In the following both errors are estimated in order to show that either effect, and thus, the total error, is small enough to be neglected.

In Fig. 5 a free body diagram of a component is shown. An increase of the velocity towards the rear of the vehicle, i.e. $v_2 > v_1$, implies that the component is compressed. With increasing compression, the amount of material which has already been decelerated to v_1 increases as well. Therefore, the boundary between the material at v_1 and the material which still exerts an inertial force against the deceleration from v_2 to v_1 moves in the negative x -direction.

The three different forces, described above, are shown in Fig. 5 as F_1 , F_2 and F_3 . The compression is caused by a force F , not necessarily in equilibrium with F_1 .

The first effect: force at the moving boundary In general, the resulting force acting upon a body is

$$\mathbf{F} = \dot{\mathbf{I}}, \tag{6}$$

with the linear momentum defined as

$$\mathbf{I} = \int_{\Omega} \rho \mathbf{v} d\Omega, \tag{7}$$

where Ω is the volume of the element in its reference configuration. ρ is the density and \mathbf{v} the velocity field. In a beam experiencing axial crushing, the velocity in the part which is already deformed is different from the velocity of the part which is still intact. Assuming the boundary between the two parts is arbitrarily sharp, each differential volume element must be either at velocity \mathbf{v}_1 or at velocity \mathbf{v}_2 , as shown in Fig. 5. Thus, with $x_{\Gamma}(t)$ being the x -position of the boundary Γ , A the cross-section in the y - z -plane and L the initial total length of the element, the element's linear momentum is

$$\mathbf{I} = \int_0^{x_{\Gamma}(t)} \int_A \rho \mathbf{v} dA dx + \int_{x_{\Gamma}(t)}^L \int_A \rho \mathbf{v} dA dx. \tag{8}$$

Differentiation with respect to time and incorporating the assumption that the velocity of any mass point is either v_1 or v_2 , yields

$$\dot{\mathbf{I}} = \frac{d}{dt} \left(\mathbf{v}_1 \int_0^{x_{\Gamma}(t)} \int_A \rho dA dx \right) + \frac{d}{dt} \left(\mathbf{v}_2 \int_{x_{\Gamma}(t)}^L \int_A \rho dA dx \right). \tag{9}$$

Under the assumption of constant cross-section A and density ρ , this becomes

$$\dot{\mathbf{I}} = \frac{d}{dt} (\mathbf{v}_1 x_{\Gamma}(t) \rho A) + \frac{d}{dt} (\mathbf{v}_2 L \rho A) - \frac{d}{dt} (\mathbf{v}_2 x_{\Gamma}(t) \rho A), \tag{10}$$

and finally

$$\dot{\mathbf{I}} = \dot{\mathbf{v}}_1 x_{\Gamma}(t) \rho A + \dot{\mathbf{v}}_2 (L - x_{\Gamma}(t)) \rho A + (\mathbf{v}_1 - \mathbf{v}_2) \dot{x}_{\Gamma}(t) \rho A. \tag{11}$$

Equation (11) can be simplified further by substituting $m_1 = x_{\Gamma}(t) \rho A$ and $m_2 = (L - x_{\Gamma}(t)) \rho A$, where m_2 is the

part of the element's mass which still needs to be decelerated and exploiting the relation $\dot{m}_1 = -\dot{m}_2$ due to constant total mass:

$$\dot{\mathbf{I}} = \dot{\mathbf{v}}_1 m_1 + \dot{\mathbf{v}}_2 m_2 + (\mathbf{v}_2 - \mathbf{v}_1) \dot{m}_2. \tag{12}$$

The difference between the section forces \mathbf{F}_1 and \mathbf{F}_2 is the force necessary to decelerate the mass of the component at the boundary Γ . With $\mathbf{F} - \mathbf{F}_1 = \dot{\mathbf{I}}$ and $\mathbf{F} - \mathbf{F}_2 = \dot{\mathbf{v}}_2 m_2$ this force is $(\mathbf{v}_2 - \mathbf{v}_1) \dot{m}_2$. For $\mathbf{v}_1 = 0$ and $\dot{\mathbf{v}}_1 = 0$, the sum of forces is reduced to

$$\dot{\mathbf{I}} = \dot{\mathbf{v}}_2 m_2 + \mathbf{v}_2 \dot{m}_2, \tag{13}$$

On a side note, the assumption $\mathbf{F}_2 = 0$, i.e. the structure does not resist deformation as, e.g., a fluid would, leads to

$$\dot{\mathbf{I}} = (\mathbf{v}_2 - \mathbf{v}_1) \dot{m}_2. \tag{14}$$

The force $\mathbf{F}_2(\mathbf{u}) = \dot{\mathbf{v}}_2 m_2$, with $\mathbf{u} = \mathbf{x}_2 - \mathbf{x}_1$, is the element's force-deformation characteristic. The remainder is the error induced by the inertia of parts of the element being decelerated at the boundary,

$$\mathbf{F}_{\text{inertia}} = \dot{m}_2 \Delta \mathbf{v}, \tag{15}$$

with the relative deformation velocity $\mathbf{v}_2 - \mathbf{v}_1 = \Delta \mathbf{v}$.

Only considering motion in the direction of x , thus reducing it to a scalar problem, with the deformation $u = x_2 - x_1$, $\frac{du}{dt} = \Delta v$ and $\frac{dm_2}{dt} = \frac{dm_2}{du} \frac{du}{dt}$, (15) is rewritten as

$$F_{\text{inertia}} = \frac{dm_2}{du} \frac{du}{dt} \Delta v = \frac{dm_2}{du} \Delta v^2. \tag{16}$$

With the assumption of constant density ρ and cross-section A , the change of mass as the boundary moves is given by

$$\frac{dm_2}{du} = \rho A. \tag{17}$$

Thus, the force necessary to decelerate the infinitesimal slabs of mass from v_2 to v_1 can be estimated by

$$F_{\text{inertia}} = \rho A \Delta v^2. \tag{18}$$

The highest possible deformation speed during a vehicle crash is given by $v_1 = 0$ and $v_2 = v_0$, where v_0 is the vehicle's initial velocity before impact, i.e. $v_0 = 15.56 \cdot 10^3 \frac{\text{mm}}{\text{s}}$ for the USNCAP crash load case (National Highway Traffic Safety Administration 2005). This gives a worst case estimate for a component which hits the barrier at the initial crash velocity. Due to the dependency on deformation speed, the error will be smaller for any component further removed from the barrier.

With the following example properties for a front rail, the set of parameters for the estimate are:

- height: $h = 140$ mm
- width: $w = 70$ mm

- sheet thickness: $t = 1.4 \text{ mm}$
- density steel: $\rho = 7.85 \frac{\text{kg}}{\text{m}^3}$
- maximum possible deformation velocity: $v_{max} = 15.56 \cdot 10^3 \frac{\text{mm}}{\text{s}}$

$F = \frac{dm}{du} v_{max}^2 = 1.12 \text{ kN}$. With, for example, a load level on the order of 100 kN, the first effect may produce an error of the order of 1 %.

The second effect: force at the right end of the component
 In order to assess the influence of the second effect, another worst case estimate is done.

The measured force-displacement-characteristic of the component is $\tilde{F}(u)$. The true force-displacement characteristic of the component is $\hat{F}(u)$, as would result when measuring during quasi-static compression. With $v_1 = 0$, and $v_2 = v_2(t)$ it follows for the force measured just on the right of the moving boundary:

$$\tilde{F}_2 = m_2 \dot{v}_2 + \hat{F}(u). \tag{19}$$

The force measured at the position x_2 , i.e. at the right end of the component, is

$$\tilde{F}_3 = \hat{F}(u). \tag{20}$$

From this

$$\frac{\tilde{F}_2}{\tilde{F}_3} = 1 + \frac{m_2 \dot{v}_2}{\hat{F}(u)} \tag{21}$$

follows for the relative error between the two measurements. Because the error depends on the acceleration, a worst case estimate for the maximum acceleration, which may occur in the vehicle structure, is necessary. Assuming the total mass of the vehicle $m = 2000 \text{ kg}$ and the maximum total force across the entire structure is $F_{tot} = 1000 \text{ kN}$, the maximum acceleration in this structure is $a_{max} = 500 \frac{\text{m}}{\text{s}^2}$. Because the effect increases with higher accelerations, a very high force was assumed. With average vehicle accelerations of between 30 g and 40 g, this provides a conservative estimate, considering the error increases with the acceleration. Given the weight of above front rail, assuming the length of the section as $L = 0.3 \text{ m}$, $m = AL\rho = 1.38 \text{ kg}$, the resulting force is 690N. Again assuming load levels on the order of 100kN, this results in an additional error on the order of less than 1 %.

Therefore the measured force-displacement characteristic is largely independent of where in between branching points it is measured. The influence of the distribution of mass in a discretized element on the force the element exerts on neighboring elements is therefore also small. Thus, any structural member is not split into more than one part unless a branching point is present such that the loads measured before and after the branching point largely differ. Any two elements with given force-displacement characteristics

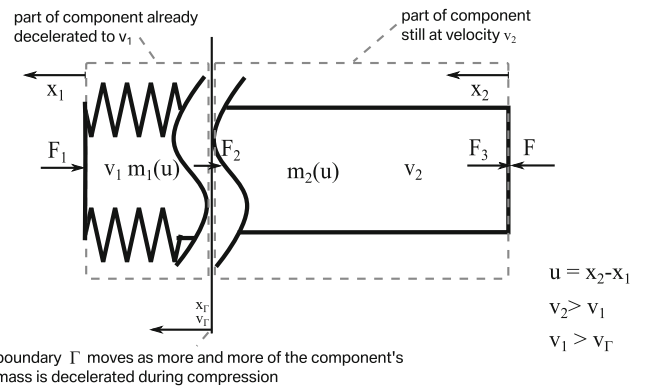


Fig. 5 A single component with a moving interior system boundary, separating active mass from already decelerated mass

which are in sequence and in between which no force is induced, can be represented by a single element. Effects of inertia, regardless of change of geometry or material along the cross-section and length of the member are neglected. This reduces the number of elements within the model to the number of free structural members and the number of nodes to the number of bifurcation points, as shown in Fig. 6.

3.4 Derivation of the force-deformation characteristics

In some cases, a reference full vehicle finite element model exists. If this is the case, the goal in building the simplified model is to obtain a model that is in good agreement with the reference model and reliably predicts the influence of design changes on the output values. For this, it is advantageous to use information, particularly the force-deformations characteristics, from the reference model.

All force-deformation characteristics which can be measured directly in the reference model, can be prescribed for the elements of the substitute model. This is done by measuring displacements and section forces of all structural members of the reference model and calculating the deformation dependent forces from that data (Fig 7). This leaves only those elements unparameterized, where the section force could not be measured, e.g. shear fields or surface structures. Figure 8 shows different classes of elements, some of which are directly measured, some calibrated and



Fig. 6 Front crash substitute model. Black dots represent branching points of the middle load path

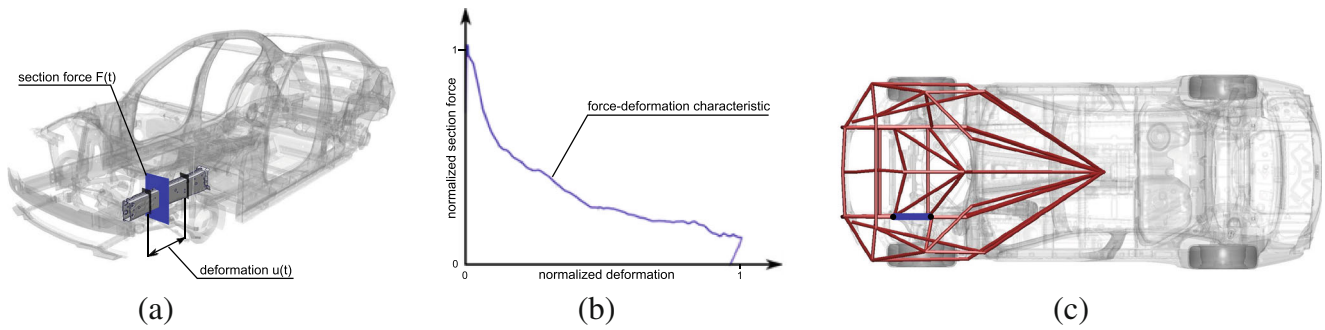


Fig. 7 A section force in the FE model (a), the measured force-deformation characteristics (b) and an element in the substitute model (c)

the remainder fixed, representing either rigid components or contact situations.

The measurable $\mathbf{F}(\mathbf{u})$ and all $\mathbf{x}(\mathbf{t} = \mathbf{0})$ and $\mathbf{u}(\mathbf{t} = \mathbf{0}) = \mathbf{0}$ are known. In order to solve (5), the mass matrix M and the initial and boundary conditions have to be defined and the unknown force-deformation-characteristics need to be identified. The latter are always the same for any single load case and can generally be prescribed beforehand. The information contained in $\mathbf{F}(\mathbf{t})$ and $\mathbf{x}(\mathbf{t})$ is used to solve for the parameters of the unknown force-deformation characteristics.

3.5 Dealing with masses and elasticities

The most relevant masses are the drive train, particularly the engine m_{eng} itself, and the rear vehicle m_{rv} . For the remaining nodal masses, it is assumed that they are each of similar magnitude and small in comparison to m_{eng} and m_{rv} . Given the mass of the entire vehicle m_{veh} , the mass for each node of the front structure is approximated as

$$m_{node} = \frac{m_{veh} - (m_{eng} + m_{rv})}{N_{nodes} - N_{nodes,engine,rv}} \tag{22}$$

In (22) the remaining mass is equally distributed among all nodes except for those already representing elements of the engine or the rear vehicle. Handling masses in this manner means that for the modeling process only m_{eng} , m_{rv} and m_{veh} need to be specified with the number of nodes and function of each node taken from the measurement definition. In case the engine and rear vehicle masses

are unknown, they are treated as calibration parameters allowed to be varied within a certain range of their assumed magnitude.

3.6 Building and solving the substitute model

Once all information needed for (5) is gathered from the reference system, the model is assembled. Any element still missing a force-deformation characteristic at this point is then parametrized for calibration using a generic, piecewise-linear force-deformation characteristic as shown in Fig. 9. The model discussed here is implemented using ABAQUS which includes an implicit solver capable of handling non-linear multi-body systems. Numerical integration of the substitute model is cheap, compared to full scale simulations, with computation times on the order of less than 10 s on a Linux workstation (2x Intel Xeon X5550, 2.67GHz, 12 GB RAM).

With all measurable $F(u)$ taken from the reference model, the parameter identification problem is finding all functions $\tilde{F}(u)$ which could not be measured. This is done using numerical optimization, which will be described in the following sections. The resulting force-deformation characteristics may exhibit, in a discretized manner, most behavior which can be found in physical components. e.g., the characteristic shown in Fig. 9 would represent a buckling of a

DESCRIPTION	EXAMPLE
MEASURED IN DETAIL MODEL	ENGINE SUPPORT BEAM
IDENTIFIED DURING CALIBRATION	FIREWALL
CONTACT DEFINITION	CONTACT ENGINE-FIREWALL
RIGID COMPONENT	ENGINE

Fig. 8 Substitute model components that are measured,calibrated, represent contact or are rigid

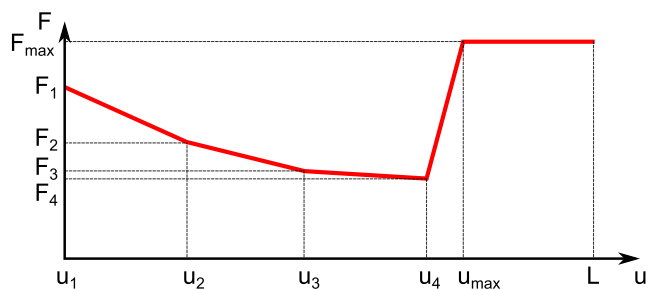


Fig. 9 Discretized force-deformation characteristic, with the support points (F_i, s_i) and a rise in load level at the length L of the structural member, representing an increase in resistance force upon densification

column type structural member, which can be seen in the initially high force level with subsequent decline. Similarly, a rather constant force-deformation characteristic would indicate some sort of axial crushing behavior or a drop of the force to zero could represent destruction of the material resulting in an elimination of the load path, as may happen with die cast or composite materials.

4 Model calibration

4.1 The optimization problem

In order to find values for the unknown model parameters, numerical optimization is used. The goal is to find the set of parameters which result in the best agreement of the simplified model with its reference model. This constitutes a parameter identification problem.

For parameter identification, the unknown force-deformation characteristics are approximated as piecewise-linear functions, as shown in Fig. 9. Degrees of freedom are the force values at the equidistant support points of the piecewise-linear functions as well as their total lengths. Fixed parameters, specified in advance, are the total possible deformations, represented by very high resistance forces upon densification, see Fig. 9. With the parameter vector $\theta = (F_1, F_2, \dots, F_j, s_j)^T$ for each component and the vector of all parameter vectors $\Theta = (\theta_1, \theta_2, \dots, \theta_i)^T$, the parameter identification problem can be written as

$$\Theta = \arg \min_{\Theta} (\Phi[\mathbf{F}_{\Theta}(\mathbf{u})]). \tag{23}$$

In (23), Φ is the *objective function*, mapping the set of system parameters to a scalar output, the error with respect to the reference model.

4.2 The objective function

Each node of the simplified model delivers an output $\hat{x}(t)$ and each element a reaction force $\hat{F}(t)$. With all $x(t)$ and a number of $F(t)$ known from the reference model for each element during a simulation, an error between estimation and reference forces and displacements can be defined as

$$e_i = \frac{1}{T \cdot f_{norm,i}} \|\Delta y_i(t)\|_2 \tag{24}$$

with

$$\Delta y_i(t) = y_i(t) - \hat{y}_i(t) \tag{25}$$

and $\|\Delta y_i\|_2 = \int_0^T (y_i(t) - \hat{y}_i(t))^2 dt$ being the L_2 -norm of the difference between estimated and reference output. y_i is either a force, displacement or acceleration, $f_{norm,i}$ is

the normalization coefficient (see Section 4.3) and T is the simulation time. In the objective function

$$\Phi = \sqrt{\frac{1}{\sum_{i=1}^n \omega_i} \sum_{i=1}^n \omega_i e_i^2} \tag{26}$$

ω_i are the weights of the respective error terms. In order to be able to evaluate multiple models, the objective function is extended by calculating the weighted L_2 -norm over all models, as shown in Fig. 10.

4.3 Normalization

Normalization is introduced in order to assure that terms of different dimension and magnitude become comparable. Normalization in the form of $\frac{\Delta y}{f_{norm}} = \frac{y - \hat{y}}{\max y}$ leads to $-1 < e_i < 1$ for deviations of less than 100 % from the reference. Normalizing in this manner leads to an objective function that is very sensitive to small absolute errors in smaller elements. For example, an element with a deformable length $L = 10 \text{ mm}$ would, with an absolute deviation of 2 mm , produce an error term of 0.2. An element with a deformable length of $L = 200 \text{ mm}$ would, with a deviation of 10 mm only produce an error 0.05. This would lead the optimization algorithm to look for solutions which even further reduce the error on the smaller element while possibly increasing the error on the larger element. To solve this problem,

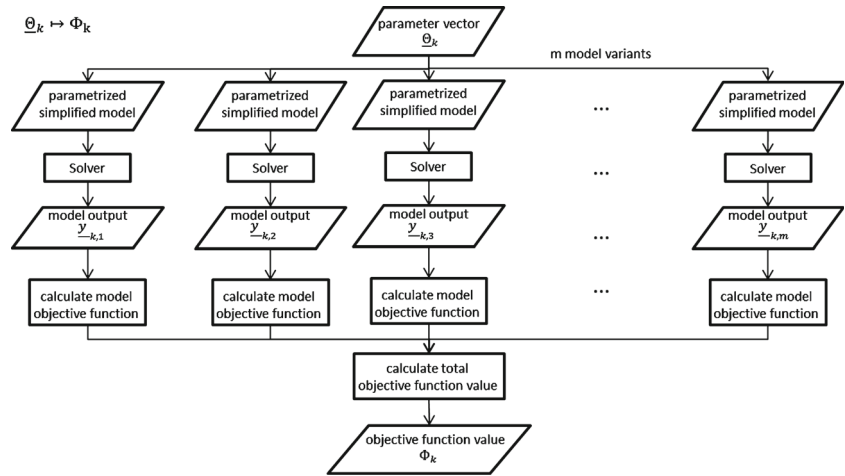
$$f_{norm} = \sqrt{\max_t y_i \cdot \max_j (\max_t y_j)} \tag{27}$$

is used to normalize forces and displacements, which introduces progressive weighting of larger elements. Accelerations are still normalized in the previous manner because no accelerations of greatly different magnitude are compared. Also, each element-wise error (24) is divided by the simulation time, in order to make simulations with different durations comparable, and the weighted L_2 -norm (26) is further divided by the sum of weights to restrict the magnitude of the error independently of the weights.

4.4 Weighting physics versus prediction

Initially, the model only produces time dependent outputs, e.g. the position of a node at time t . The design target values, such as maximum acceleration and firewall intrusions, are time independent values and have to be derived from the time dependent outputs. Considering only time-dependent quantities for calibration may put the focus on details that are not important for the prediction of the time-independent

Fig. 10 Workflow of the objective function evaluation for a single parameter vector using multiple models. All models are evaluated with the same calibration parameters and the objective function is calculated for each model and then over all models



variables, which are of interest. Therefore, it is of interest to directly consider the scalar quantities in the objective function. Thus we want to distinguish contributions to the objective function: deviations of time dependent quantities and time independent quantities. The first we call physical, because they represent the mechanical state of the model in terms of forces, displacements and their derivatives. The second we call predictive, because they are the values the model is supposed to predict for evaluation in terms of crashworthiness, independently of a correct representation of the physical details. This approach results in a new objective function,

$$\Phi^* = \sqrt{\sum_{j=1}^m (\beta \Phi_j^2 + (1 - \beta) \Psi_j^2)} \tag{28}$$

which is the L_2 -norm of deviations from the reference state over all models, $j = 1, 2, \dots, m$, and which includes additionally the prediction capability of the model with respect to all targets (maximum acceleration and intrusion). Here the additionally considered target values, accelerations and intrusions, are represented by the term

$$\Psi = \sqrt{\sum_{k=0}^p \gamma_k \psi_k^2}, \tag{29}$$

with the contribution of the accelerations

$$\psi_0 = \frac{\max(a(t)) - \max(\hat{a}(t))}{\max(a(t))} \tag{30}$$

and the contribution of the intrusions

$$\psi_k = \frac{u_k(t_{end}) - \hat{u}_k(t_{end})}{u_k(t_{end})}, \tag{31}$$

for $k = 1, 2, \dots, p$, with p as the number of points where intrusion u_k is measured, each of which weighted by γ_k . Equation (29) is the prediction error

for one model and in (28) β is the relative weight between prediction of target values and agreement of the physical response with the respective reference system. Equation (30) is the prediction error of the maximum of the filtered acceleration and (31), for $k > 0$, is the prediction error of the static firewall intrusion at the k th point of the firewall.

With $0 \leq \beta \leq 1$, β determines how much the objective function focuses on the scalar prediction values and how much it focuses on a good agreement between the time-dependent outputs of the models. Thereby, it directly controls the agreement of model output and training data as well as the robustness regarding unknown variations, see Fig. 11. A better agreement of the time-dependent quantities usually yields a more robust model while a better fit to the known predictions may cause less deviation from the reference with respect to variations within the range of the models used for calibration. It is important to note that robustness usually comes at the cost of predictive quality with respect to the calibration models. Increasing β , i.e. increasing the weight of the time-dependent system states, will worsen the immediate results of calibration. In turn, unknown configurations are more likely to be correctly predicted. The objective function always penalizes both, errors in transient and predicted variables, weighted by β and $1 - \beta$ respectively.

4.5 The optimization algorithm

The optimization problem is non-linear, non-convex, e.g. because the model’s contact definitions resemble step-functions. The discontinuous properties of Φ make the use of linear or quadratic programming or gradient based optimization algorithms difficult. Also, depending on the level of detail of the substitute model and the discretization of the unknown force-deformation characteristics, the dimension-

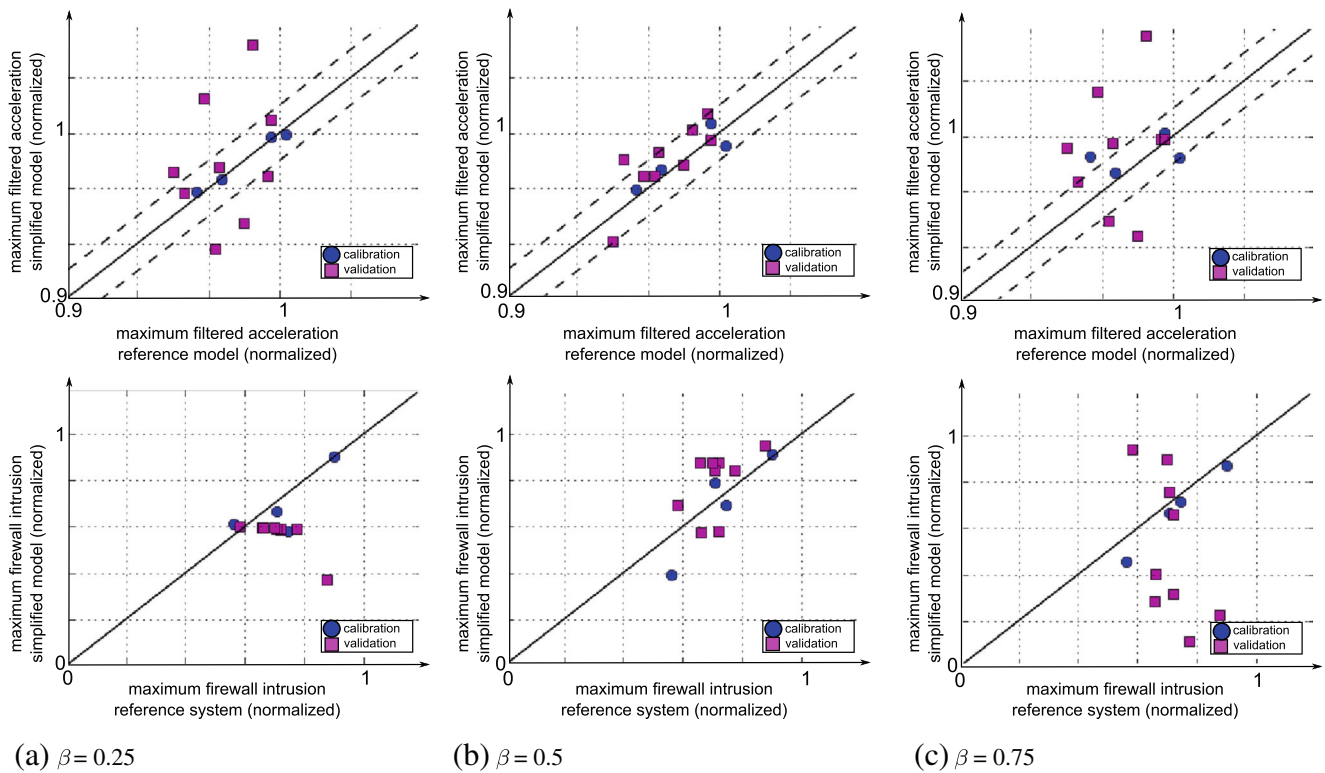


Fig. 11 Calibration and validation results for (a) low β (weight on prediction), (b) high β (weight on physics), and (c) $\beta = 0.5$ (balanced)

ality of the parameter space is high, in general on the order of $p = 100$. This makes the numerical estimation of the jacobian J and hessian H costly at $N + 1$ and $2N + 1$ sample points respectively. Analytical estimates for J and H cannot be given. Simplex algorithms tend to not perform well on higher dimensional problems. These properties make evolutionary or genetic algorithms the methods best suited for the task.

From the array of evolutionary and genetic algorithms adaptive simulated annealing, self adaptive evolution, efficient global optimization and differential evolution were tested. Due to its analogy to a physical system’s sequential states, adaptive simulated annealing does not easily support parallel computing (Ingber 1996). Although there are parallel implementations of the algorithm, the code available during this project does not support parallel computation of sample points. Despite having a reputation for converging fast, the lack of parallel submission of calculations puts it behind other stochastic algorithms in testing. Response surface based optimization algorithms, like efficient global optimization, support parallel computing for the initial design of experiments for the base response surface, which is then iteratively refined with each function evaluation. The refinement process is not suited for parallel function evaluations because the parameters for each new sample point are determined based on the current response surface built

from all previous points. Amongst self adaptive evolution and differential evolution, (Storn and Price 1997), the latter outperformed self adaptive evolution in every try, e.g., see Fig. 12. Simulated Annealing was unable to get past the second iteration in the given time due to the lack of parallel computing in the given implementation. Differential evolution is explicitly tailored to support parallel computing and facilitates such by providing constant population sizes and parameter vector dimensions over the course of the entire optimization. The authors of Storn and Price (1997) also state that the convergence of the differential evolution algorithm has been empirically found to show no substantial improvements for raising the population size above about 40, independent of the number of parameters, as explained in Storn and Price (2013). The new population is generated from the current population depending on the parameters F and CR . F determines how far a new sample point may lie from its base point and CR determines the probability that components of a newly generated point make it into the next population, which is called crossover. The parameters for the optimization algorithm were based on the advice given in Storn and Price (2013), and thus set as follows:

- Crossover ratio $CR = 0.9$,
- Weighting factor $F = 0.8$,
- Populations size $NP = 48$.

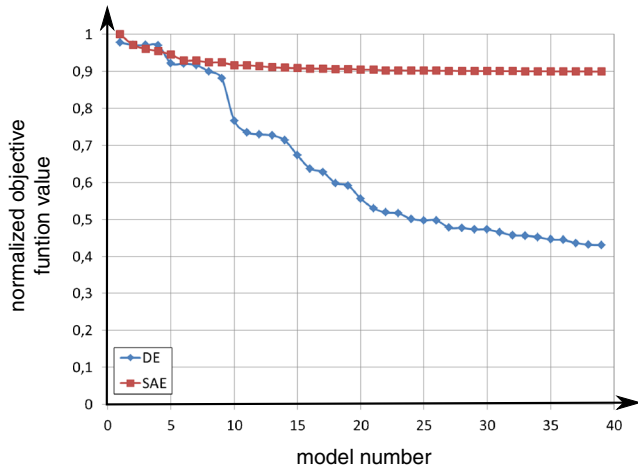
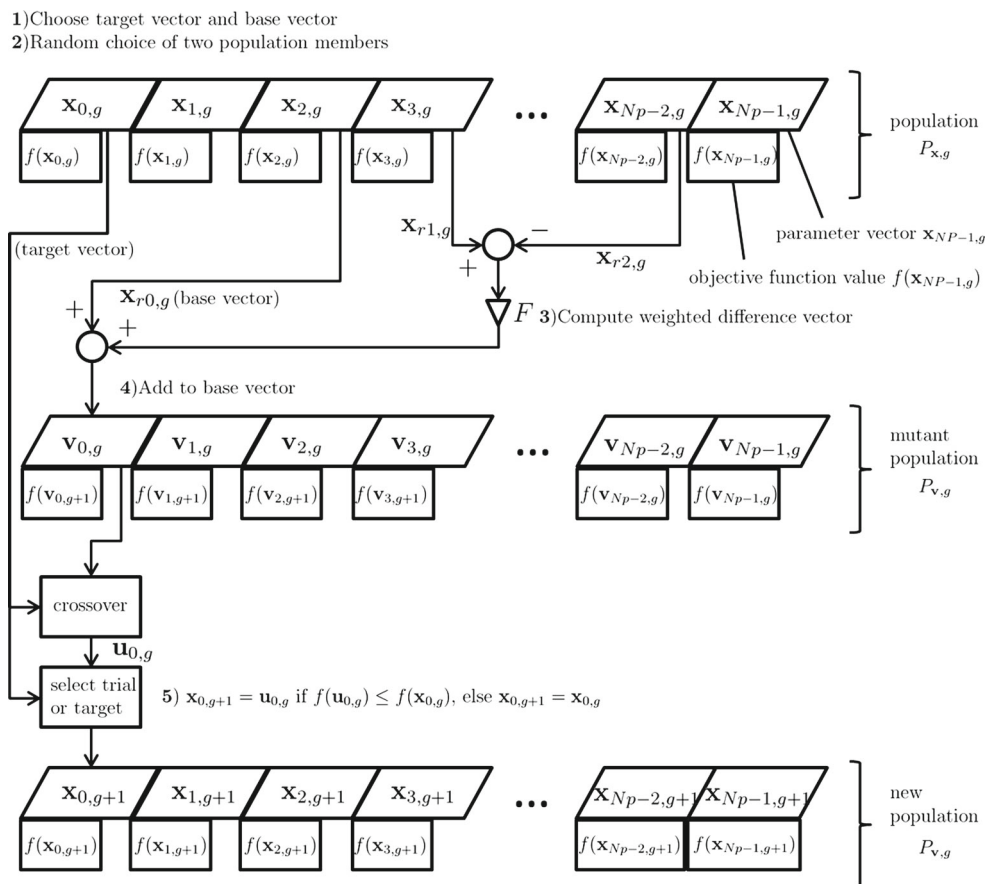


Fig. 12 Comparison of Differential Evolution (DE) with self adaptive evolution (SAE) over the course of 39 iterations

The choice of $NP = 48$ is based on above statement and the desire to have a multiple of 12, as this is number of cores available on the workstation used, which facilitates parallel computation of sample points. In Fig. 13, the differential evolution scheme is illustrated (see Storn and Price 2013).

Fig. 13 Workflow of the differential evolution algorithm, according to Storn and Price (2013)



4.6 Single model parameter identification

Usually when building a simplified, physics based model of a system, the parameters of the model are chosen such that it is in good agreement with its reference system. Figure 15a shows the output of the maximum filtered acceleration of the reference and substitute model under variation of design parameters. While the output deviates less than 2% from the calibration design, variations in design parameters, which cause the acceleration to deviate from this point can not be correctly predicted. The prediction does not only fail in terms of magnitude but also in terms of relative prediction, meaning that a design variation which causes the pulse to rise in the reference system should also cause the predicted pulse to rise. This is not given as shown by the points forming clusters oriented orthogonal to the main diagonal, rather than parallel to it.

4.7 Multiple model parameter identification

For better results, a multiple model approach to parameter identification is chosen. While the solution to the single-model parameter identification problem is not unique given a single load case and configuration of measured parame-

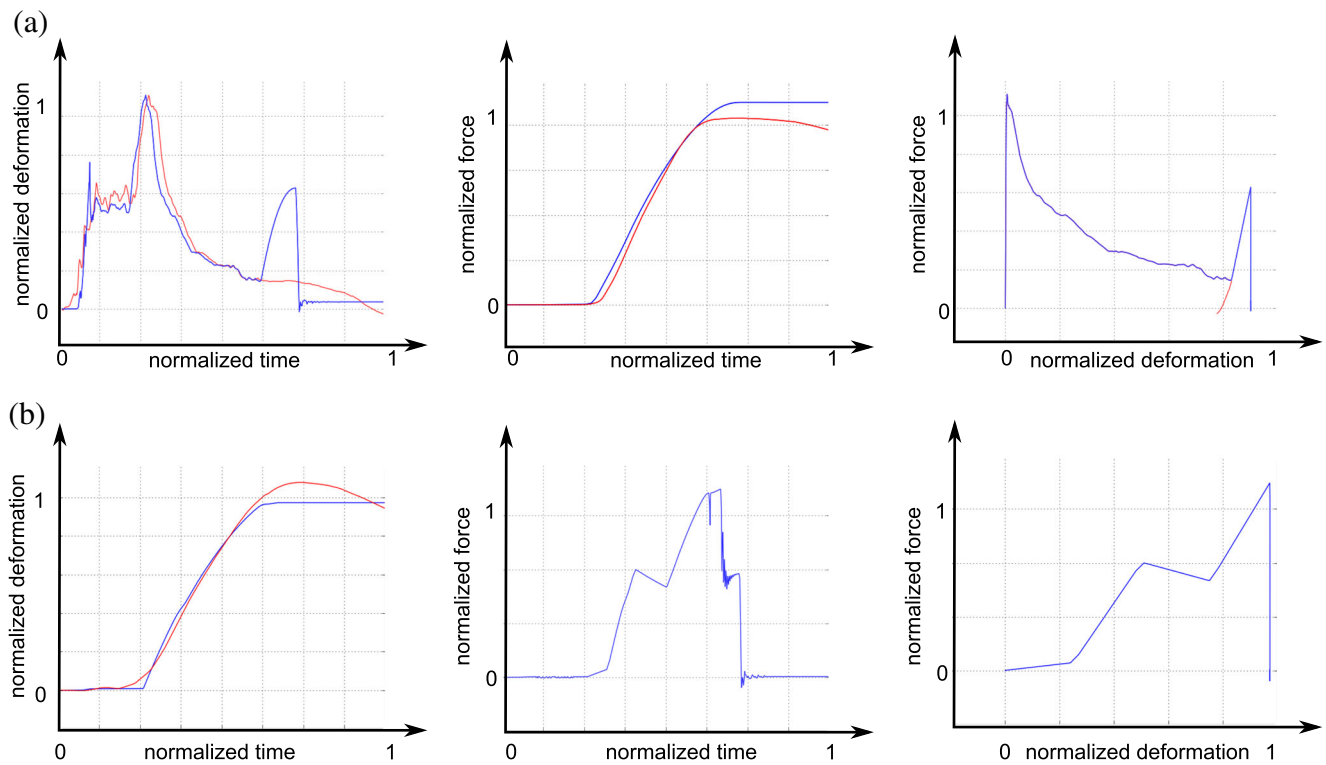


Fig. 14 $F(t)$, $u(t)$ and $F(u)$ for a measured component, the front rail (a), and a calibrated component, the wheel (b), after calibration

ters, the number of solutions, which minimize Φ for each model with varying measured parameters and therefore also varying loads on the elements with unknown parameters, is much smaller. It becomes more probable to find a set of parameters which also satisfies unknown model configurations, the more different models and reference systems are used for calibration, see Fig. 15.

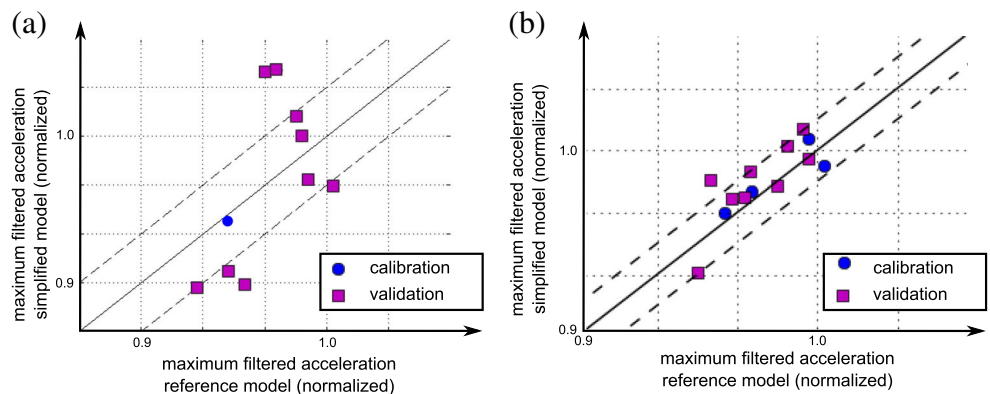
Figure 14 shows that the displacements and forces of a single model are in good agreement with the reference model after multi-model parameter identification.

Model evaluation is now done differently from the single-model parameter identification problem. An array of models is used for calibration and cross validation, such that the

predictive qualities of the model with respect to changes in design parameters can be evaluated as well as the models physical output agreement with each reference model (Fig. 15). Once a set of parameters which produces sufficiently good results in cross validation as well as physical output agreement is found, this set can be incorporated into the model. This model is then already explicitly validated against unknown design parameter changes through the cross validation process.

In contrast to Fig. 15a, b shows that the model calibrated using multiple reference systems produces prediction errors in the magnitude of less than 1g, which is less than 3%. Also, its relative predictions are superior to those made by

Fig. 15 Calibrating with respect to several models improves results for the validation sample over the calibration taking into account only one model. The R^2 values are computed only using the cross-validation sample points



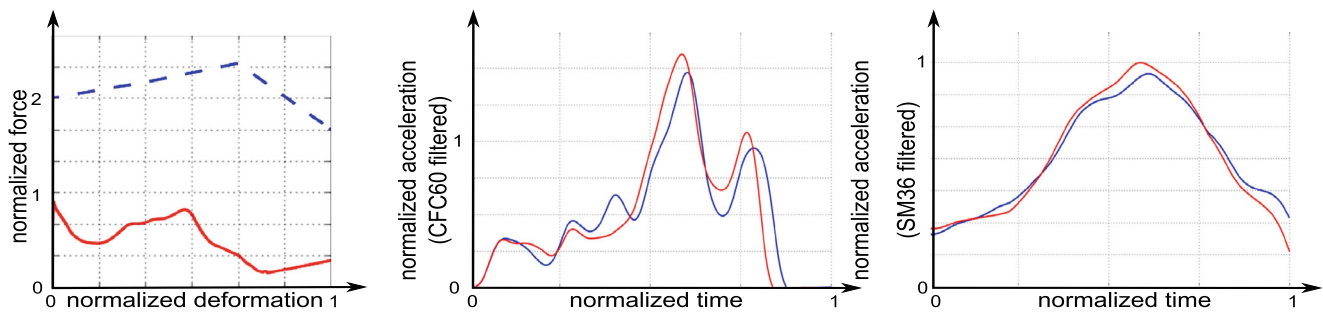


Fig. 16 Influence of front-rail modification (*dashed line*) of a nominal design (*solid line*): (*left*) force-deformation characteristic, (*middle*) acceleration with cfc60 filter, (*right*) acceleration with sm36 filter

the model calibrated with respect to only a single reference system. This also becomes clear when looking at the coefficient of determination for the cross-validation sample points only, which is $R^2 = 0.74$ for the multi-model calibration as opposed to $R^2 = 0.37$ when using a single reference model.

5 Application of the substitute model

One possible application for a substitute model is the quick assessment of design variants. Here, an example variation of the load level of the front rail and its influence on the resulting B-pillar acceleration is shown (Fig. 16). By raising the load level of a component that contributes to the deceleration of the vehicle at an early time during the crash, e.g. the front rail, as shown in Fig. 16, more energy is dissipated early on. This leads to lower velocities during a phase of large deformation and thereby to lower final accelerations as the vehicle reaches a halt. This mechanism is correctly reproduced in the substitute model.

In this manner it is possible to quickly assess changes in components load levels and their respective effect on crash performance. Therefore, the model is well suited for optimization or stochastic analyses. For example, using stochastic methods, see Lehar and Zimmermann (2011), thousands of model evaluations can be performed in order to identify a feasible solution space for the design parameters, in this case the load levels of each component. These intervals, defined for the force-deformation characteristic of each component, then define goals for component development.

6 Limitations

Regarding the limitations of the model, the following has to be noted. A correct physical representation of components is only given for those components whose force-deformation characteristics were taken directly from the reference FE model. The force-deformation characteristic of a calibrated

component may lie in the vicinity of the component's true physical behavior. However, this cannot be verified because the force-deformation characteristics of components which are calibrated cannot be measured in the reference model. Also, parameters identified by optimization may compensate for errors induced by the assumptions and simplifications made.

While the approach presented in this work is currently only implemented and validated for the USNCAP, extensions for other load cases are considered possible. Load cases with deformable crash barriers require an adequate simplified model of the barrier. Load cases with a movable crash barrier require a different approach for linear momentum, i.e., two masses have to be considered. Also, the approach is appropriate only for components that are loaded only in the x -direction.

Whenever the assumptions made in this work are valid, however, the approach is recommended as it provides high accuracy at relatively low modeling effort and computational cost while reducing the problem to its design-relevant functional parameters.

7 Conclusion

In this work, an approach for substitute modeling was formulated which tackles some persistent issues in substitute modeling of crash problems.

Initially, a set of concept variables most suited for describing the functional properties of the crash structure was identified. It was shown that the functional properties of this structure are the force response of the front vehicle at any given deformation. This force in turn is the sum of all forces acting in parallel at the given deformation.

For the calibration process, progressive normalization, taking into account the large differences in the maximum deformations of elements, was introduced. This ensures that the optimization weights for the elements can be chosen independent of the elements' lengths.

The problem of uncertain predictive qualities was addressed by *multiple model calibration* and cross validation of the substitute model with several reference designs. This greatly improves the prediction of the response of the crash structure to changes in the structural components.

A hybrid calibration process is introduced which distinguishes between integrated output values and the agreement of the substitute model with the reference system's physical states. This makes it possible to shift the focus of the calibration toward better prediction of the integrated output quantities at the cost of the agreement of its time-dependent states. In combination with the multiple model calibration, robust and precise predictions of filtered maximum accelerations and intrusions using a computationally comparatively cheap model are achieved.

References

- Carvalho M, Ambrosio J, Eberhard P (2011) Identification of validated multibody vehicle models for crash analysis using a hybrid optimization procedure. *Struct Multidiscip Optim* 44(1):85–97. doi:[10.1007/s00158-010-0590-y](https://doi.org/10.1007/s00158-010-0590-y)
- Cornette D, Thirion JL, Bos F, Dittlo M, Lorriliere F, Drazetic P, Markiewicz E, Payen F (1997) Plastic hinge concept for simplified vehicle crash simulation. Automotive Automation Limited, England
- Duddeck F (2008) Multidisciplinary optimization of car bodies. *Struct Multidiscip Optim* 35:375–389
- Halgrin J, Haugou G, Markiewicz E (2008) Integrated simplified crash modelling approach dedicated to pre-design stage: evaluation on a front car part. *Int J Veh Saf* 3(1):91–115
- Hollowell WT (1986) Adaptive time domain, constrained system identification of nonlinear structures. University of Virginia, Charlottesville, USA. <http://books.google.de/books?id=Ds3gNwAACAAJ>
- Huang M (2002) Vehicle crash mechanics. CRC Press LLC, Boca Raton
- Ingber L (1996) Adaptive simulated annealing (asa): Lessons learned. Lester Ingber Papers 96as, Lester Ingber. <http://ideas.repec.org/p/lei/ingber/96as.html>
- Kamal MM (1970) Analysis and simulation of vehicle to barrier impact. SAE paper 700414
- Kerstan H, Bartelheimer W (2011) Innovative Prozesse und Methoden in der Funktionsauslegung - Auslegung fuer den Frontcrash. VDI-Berichte 2078:185–196
- Kim C, Arora J (2001) Nonlinear dynamic system identification for automotive crash using optimization: a review. *Struct Multidiscip Optim* 25(1):2–18. doi:[10.1007/s00158-002-0267-2](https://doi.org/10.1007/s00158-002-0267-2)
- Kim C, Mijar A, Arora J (2001) Development of simplified models for design and optimization of automotive structures for crashworthiness. *Struct Multidiscip Optim* 22(4):307–321. doi:[10.1007/PL00013285](https://doi.org/10.1007/PL00013285)
- Lehar M, Zimmermann M (2011) An inexpensive estimate of failure probability for high-dimensional systems with uncertainty (*Struct Saf* (2011) doi:[10.1016/j.strusafe.2011.10.001](https://doi.org/10.1016/j.strusafe.2011.10.001))
- Markiewicz E, Marchand M, Ducrocq P (2001) Evaluation of different simplified crash models: application to the under-frame of a railway driver's cab. Inderscience Publishers
- National Highway Traffic Safety Administration (2005) Office of vehicle safety compliance, room 6111, NVS-220, 400 Seventh Street, SW Washington, DC 20590: TP208-13 laboratory test procedure
- Nikraves PE, Chung IS, Benedict RL (1983) Plastic hinge approach to vehicle simulation using a plastic hinge technique. *Comput Struct* 16:395–400
- Pereira MS, Ambrósio J (1997) Crashworthiness analysis and design using rigid-flexible multibody dynamics with application to train vehicles. *Int J Numer Methods Eng* 40(4):655–687
- Sousa L, Verssimo P, Ambrósio J (2008) Development of generic multibody road vehicle models for crashworthiness. *Multibody Syst Dynamics*
- Storn R, Price K (2013) Differential evolution homepage. <http://www1.icsi.berkeley.edu/storn/code.html>
- Storn R, Price K (1997) Differential evolution - a simple and efficient heuristic for global optimization over continuous spaces. *J Glob Optim* 11:341–359
- Wieggers KE (2003) Software Requirements. Microsoft Press, Redmond